Relativistic mean field study of light medium nuclei away from beta stability

S. K. Patra and C. R. Praharaj
Institute of Physics, Bhubaneswar–751 005, India
(Received 12 March 1991)

Bulk properties like binding energies, rms radii, and quadrupole deformations of Ca, Ti, Cr, Fe, Ni, and Zn nuclei are calculated in the deformed relativistic mean field model. Excellent results for the experimentally known binding energies and radii of nuclei are obtained. The calculation is extended to nuclei near the neutron-drip line. Dips in quadrupole deformation are seen for the known closed-shell configurations and enhanced deformations are obtained for specific neutron numbers.

I. INTRODUCTION

The properties of nuclei away from the valley of β stability is a topic of much current interest [12,13,15]. The study of such exotic nuclei can serve to put constraints on the parameters of the effective nuclear interaction, which is responsible for the binding of such nuclei and their other properties, such as their radii, shapes, and deformations. Estimates of the masses of such nuclei can be made by extrapolation of various mass formulas [19]. At a microscopic level the binding energies of nuclei can be calculated using effective interactions of the Skyrme type [20]. Recently attempts have been made to study the effective interactions in finite nuclei using Dirac-Hartree-Fock equations starting with boson exchange two-nucleon interactions [28,29].

In recent years great progress has been made in gaining a microscopic understanding of various nuclear properties starting with interacting nucleon and meson fields in a relativistic framework [2,16,17,21–23]. Solutions of the self-consistent relativistic mean field (RMF) equations for nucleons and mesons (in the relativistic Hartree-Fock approximation) provide a basis for studying the nuclear ground-state properties. A distinct advantage is that, with proper relativistic kinematics and with the mesons and their properties already known or fixed from the properties of a small number of finite nuclei [4], the method gives excellent results for the binding energies and other properties of not only the spherical nuclei, but also of some well-known deformed nuclei. The parameters sets also describe the nuclear matter properties well. The quality of agreement with the known binding energies of nuclei is better than that obtained in mean field calculations using Skyrme-type effective interactions. Another attractive feature of the relativistic mean field approach is that the spin-orbit interaction and the associated nuclear shell model come out naturally as arising from meson-nucleon interactions [2,25].

Relativistic mean field (RMF) models thus have something useful to say about the binding energies and other bulk properties of known nuclei [2,5] and it would be interesting to extend the RMF calculations to nuclei near the neutron-drip line. Also the investigation of the rms radii of neutron-rich nuclei and possible neutron halos [12,13,15,36] remains a current experimental and theoretical topic and RMF studies can help to enhance our understanding of this aspect.

In this work we have undertaken a study of some of these quantities for the even-even $Z=20-30$ nuclei using the RMF theories developed by Walecka, and others [1,2,3,6,18]. The modification suggested by Boguta and Bodmer [6] is to add nonlinear terms to the potential in which the σ meson moves. This gives a better value for the bulk compressibility modulus in nuclear matter than the original Walecka model. In this paper we work with the nonlinear model of Boguta and Bodmer. Recently Zimanyi and Moszkowski [8] have proposed a derivative scalar coupling model to account for the effective mass and the compressibility modulus.

Some of these $Z=20-30$ even-even nuclei may not be spherical and we use the deformed relativistic mean field method given by Gambhir, Ring, and Thimet [5] and Price and Walker [7]. The deformed mean field method is general enough that both deformed and spherical nuclei can be studied. We study chains of isotopes of a given Z till the neutron-drip line using σ, ω, ρ, and the photon as the bosons mediating the interaction among nucleons. It is known that the ρ meson (an isovector) couples to the isospin of the nucleons [3,4]. The ρ meson is thus important for the binding of neutron-rich (or proton-rich) nuclei (i.e., nuclei with finite isospin quantum numbers in the ground state) and hence for the location of the neutron-drip (proton-drip) line.

The RMF has in-built the right spin-orbit interaction and hence the nuclear shell effect and the symmetry energy term of the nuclear binding (coupling with ρ meson) and can give reliable predictions of various nuclear properties (binding energies, shape, and sizes) and the neutron-drip (proton-drip) lines starting from interacting mesons and nucleons. This is important if one is calculating for nuclei far from the valley of stability (as we are doing here for nuclei near the neutron-drip line), where extrapolation of mass formulas may not be very reliable.

The paper is organized as follows. In Sec. II we present the equations for the nucleon and meson fields used in this work and the method of solution of these equations. The properties of the various mesons and their couplings are briefly given in Sec. III. In Sec. IV we

present the results of our calculation for the binding energies, radii, deformations, and the shell closures and compare these with experiments and other theoretical studies wherever possible. Predictions for the neutron-drip line, quadrupole deformation, rms radii, spin-orbit splitting, and deformed configurations in traditional spherical closed-shell nuclei are given in this section. The concluding remarks are given in Sec. V. In the Appendix we discuss about the tensor coupling of vector mesons and show that it does not contribute to the mean-field equations of even-even nuclei.

II. RELATIVISTIC LAGRANGIAN AND RMF APPROXIMATION FORMALISM

The relativistic Lagrangian density is given by [2,5]

$$\begin{aligned}\mathcal{L}=&\bar{\psi}_i\{i\gamma^\mu\partial_\mu-M\}\psi_i+\tfrac{1}{2}\partial^\mu\sigma\partial_\mu\sigma-U(\sigma)\\&-g_s\bar{\psi}_i\psi_i\sigma-\tfrac{1}{4}\Omega^{\mu\nu}\Omega_{\mu\nu}+\tfrac{1}{2}m_w^2V^\mu V_\mu-g_w\bar{\psi}_i\gamma^\mu\psi_iV_\mu\\&-\tfrac{1}{4}\vec{B}^{\,\mu\nu}\vec{B}_{\mu\nu}+\tfrac{1}{2}m_\rho^2\vec{\rho}^{\,\mu}\vec{\rho}_\mu-g_\rho\bar{\psi}_i\gamma^\mu\vec{\tau}\psi_i\vec{\rho}_\mu\\&-\tfrac{1}{4}F^{\mu\nu}F_{\mu\nu}-e\bar{\psi}_i\gamma^\mu\frac{(1-\tau_{3i})}{2}\psi_iA_\mu\ .\end{aligned}\tag{1}$$

The field for the σ meson is denoted by σ, that of the ω meson by V_μ, and of the ρ meson by $\vec{\rho}_\mu$. The arrow in the $\vec{\rho}$ field denotes its isovector character. A^μ denotes the electromagnetic field, which couples to the protons. ψ are the Dirac spinors for the nucleons, whose third components of isospin are denoted by τ_3. We use the convention that the eigenvalue t_i of τ_{3i} for a neutron is $+\frac{1}{2}$ and for a proton it is $-\frac{1}{2}$. Here g_s, g_w, g_ρ, and $e^2/4\pi$ are the coupling constants for σ, ω, ρ mesons, and photon, respectively. M is the mass of the nucleon and m_σ, m_ω, and m_ρ are the masses of the σ, ω, and ρ mesons, respectively.

According to Boguta and Bodmer [6] the σ mesons move in a nonlinear potential with interaction among themselves. Therefore the potential of σ field $U(\sigma)$ is expressed as

$$U(\sigma)=\tfrac{1}{2}m_\sigma\sigma^2+\tfrac{1}{3}g_2\sigma^3+\tfrac{1}{4}g_3\sigma^4\ .\tag{2}$$

In the original Walecka model the bulk modulus K was found to be 560 MeV, whereas the empirical value is 210±30 MeV [43]. With the above nonlinear sigma potential, the bulk modulus was found to be $K\approx212$ MeV. (Other properties using nonlinear sigma model are given in Sec. III.) We use this nonlinear model in this work. The field tensors for the vector mesons and the electromagnetic field are defined as

$$\vec{B}^{\,\mu\nu}=\partial^\mu\vec{\rho}^{\,\nu}-\partial^\nu\vec{\rho}^{\,\mu}-g_\rho(\vec{\rho}^{\,\mu}\times\vec{\rho}^{\,\nu})\ ,\tag{3a}$$

$$\Omega^{\mu\nu}=\partial^\mu V^\nu-\partial^\nu V^\mu\ ,\tag{3b}$$

$$F^{\mu\nu}=\partial^\mu A^\nu-\partial^\nu A^\mu\ .\tag{3c}$$

To describe the ground-state properties we need a static solution of the above Lagrangian. For this case the meson and electromagnetic fields are time independent, whereas the nucleon wave functions oscillate with single-particle energy E_i. Further due to time-reversal symmetry the vector (spatial) parts of the vector potentials V and ρ, and of the electromagnetic potential A vanish. The charge conservation implies that only the third component of the isovector vector field ρ_0 contributes to the interaction with nucleons. Under this condition the Dirac equation for the nucleons and the Klein-Gordon equation for bosons become [2]

$$[-i\vec{\alpha}\cdot\vec{\nabla}+\beta M(r)^*+V(r)]\psi_i(r)=E_i\psi_i(r)\ .\tag{4a}$$

We have neglected the contribution of antiparticles [2]. Here $M(r)^*=M+g_s\sigma(r)$ is the effective mass of the nucleon, which is significantly smaller and space dependent because of the σ-meson field. The equations satisfied by the boson fields are

$$\frac{d^2\sigma(r)}{dr^2}+\frac{2}{r}\frac{d\sigma(r)}{dr}-m_\sigma\sigma(r)=g_s\rho_s(r)+g_2\sigma^2(r)+g_3\sigma^3(r)\ ,\tag{4b}$$

$$\frac{d^2V_0(r)}{dr^2}+\frac{2}{r}\frac{dV_0(r)}{dr}-m_\omega V_0(r)=-g_\omega\rho_v(r)\ ,\tag{4c}$$

$$\frac{d^2\rho_0(r)}{dr^2}+\frac{2}{r}\frac{d\rho_0(r)}{dr}-m_\rho\rho_0(r)=-g_\rho\rho_\rho(r)\ ,\tag{4d}$$

$$\frac{d^2A_0(r)}{dr^2}+\frac{2}{r}\frac{dA_0(r)}{dr}=-e\rho_c(r)\ .\tag{4e}$$

Here

$$\rho_s(r)=\sum_{i=1}^{A}\bar{\psi}_i(r)\psi_i(r)\tag{5a}$$

is the Lorentz-scalar density,

$$\rho_v(r)=\sum_{i=1}^{A}\bar{\psi}_i(r)\gamma^0\psi_i(r)\tag{5b}$$

the baryonic density,

$$\rho_\rho(r)=\sum_{i=1}^{A}\bar{\psi}_i(r)\gamma^0\tau_{3i}\psi_i(r)\tag{5c}$$

the isovector density, and

$$\rho_c(r)=\sum_{i=1}^{A}\bar{\psi}_i(r)\gamma^0\frac{(1-\tau_{3i})}{2}\psi_i(r)\tag{5d}$$

the proton density

$$V(r)=g_\omega V_0(r)+g_\rho\tau_3\rho_0(r)+e\frac{(1-\tau_3)}{2}A_0(r)\ .\tag{5e}$$

(i) Spherical nuclei

The densities and the potentials have spherical symmetry and the single-particle wave function ψ_i in a central parity conserving field is written as

$$\psi_i(r,t)=\begin{bmatrix}f_i(r)\mathcal{Y}_{l_ij_im_i}\\ ig_i(r)\mathcal{Y}_{\bar{l}_i\bar{j}_im_i}\end{bmatrix}\chi_{t_i}(t)\ ,\tag{6}$$

where $l=j\pm\frac{1}{2}$, $\bar{l}=j\mp\frac{1}{2}$ and $f_i(r)$ and $g_i(r)$ are the upper and lower components of the Dirac spinor, respectively, and the $\mathcal{Y}$ are the spin-angle functions [34].

Substituting the value of ψ_i of Eq. (6) in the set of Eq. (4) the Dirac equation splits into two first-order differential equations, and the ρ's are written in terms of $f_i(r)$ and $g_i(r)$:

$$[M(r)^*+V(r)]f_i(r)+\left[\partial_r-\frac{k_i-1}{r}\right]g_i(r)=E_i f_i(r)\ , \quad (7a)$$

$$-[M(r)^*-V(r)]g_i(r)-\left[\partial_r+\frac{k_i+1}{r}\right]f_i(r)=E_i g_i(r)\ , \quad (7b)$$

and the densities become

$$\rho_s(r)=\sum_i n_i(2j_i+1)[|f_i(r)|^2-|g_i(r)|^2]\ , \quad (8a)$$

$$\rho_v(r)=\sum_i n_i(2j_i+1)[|f_i(r)|^2+|g_i(r)|^2]\ , \quad (8b)$$

$$\rho_\rho(r)=\sum_i 2n_i t_i(2j_i+1)[|f_i(r)|^2+|g_i(r)|^2]\ , \quad (8c)$$

$$\rho_c(r)=\sum_i n_i(\tfrac{1}{2}-t_i)(2j_i+1)[|f_i(r)|^2+|g_i(r)|^2]\ , \quad (8d)$$

where $k_i=\pm(j_i+\frac{1}{2})$ for $j_i=l_i\mp\frac{1}{2}$ and, the occupation number $n_i=1$ *for occupied level,* 0 *for unoccupied level.*

(ii) Deformed nuclei and symmetries of the mean field

For deformed nuclei, the potentials in which a nucleon moves are not spherically symmetric. Though spherical symmetry is absent, we assume that the potentials and densities have axially symmetric shapes. In this situation the source terms in the Dirac and Klein-Gordon equations are not spherically symmetric, but are deformed (with axial symmetry). Hence for deformed nuclei we have to modify the above equations taking into account the axially symmetric shapes. In this case the rotational symmetry is broken and therefore j is no longer a good quantum number, but the densities are still invariant with respect to a rotation around the symmetry axis. We have to work with the cylindrical coordinates [5]

$$x=r_\perp\cos\varphi\ , \quad (9a)$$

$$y=r_\perp\sin\varphi\ , \quad (9b)$$

$$z=z\ . \quad (9c)$$

The projection of angular momentum along the symmetry axis is a good quantum number. Hence Dirac spinor ψ_i can be written as

$$\psi_i(\vec{r},t)=\frac{1}{\sqrt{2\pi}}\begin{bmatrix} f_i(z,r_\perp)^+\exp i(\Omega_i-\frac{1}{2})\varphi \\ f_i(z,r_\perp)^-\exp i(\Omega_i+\frac{1}{2})\varphi \\ ig_i(z,r_\perp)^+\exp i(\Omega_i-\frac{1}{2})\varphi \\ ig_i(z,r_\perp)^-\exp i(\Omega_i+\frac{1}{2})\varphi \end{bmatrix}\chi_{t_i}(t)\ . \quad (10)$$

Substituting the value of ψ_i from Eq. (10) in Eqs. (4) we get

$$(M^*+V)f_i^+ +\partial_z g_i^+ +\left[\partial_{r\perp}+\frac{\Omega+1/2}{r_\perp}\right]g_i^-=E_i f_i^+\ , \quad (11a)$$

$$(M^*+V)f_i^- -\partial_z g_i^- \left[\partial_{r\perp}-\frac{\Omega-1/2}{r_\perp}\right]g_i^+=E_i f_i^-\ , \quad (11b)$$

$$(M^*-V)g_i^+ +\partial_z f_i^+ +\left[\partial_{r\perp}+\frac{\Omega+1/2}{r_\perp}\right]f_i^-=-E_i g_i^+\ , \quad (11c)$$

$$(M^*-V)g_i^- -\partial_z f_i^- +\left[\partial_{r\perp}-\frac{\Omega-1/2}{r_\perp}\right]f_i^+=-E_i g_i^-\ , \quad (11d)$$

and the Klein-Gordon equations become

$$\left[-\frac{1}{r_\perp}\partial_{r\perp}r_\perp\partial_{r\perp}-\partial_z^2+m^2_{\text{boson}}\right]\phi(\text{boson}(r_\perp,z)) =\text{source terms}\ . \quad (12a)$$

In Eq. (12a) we have, in the source terms, the densities

$$\rho_{s,v}(r_\perp,z)=2\sum_{i>0} n_i[(|f_i^+|^2+|f_i^-|^2)\mp(|g_i^+|^2+|g_i^-|^2)]\ , \quad (12b)$$

$$\rho_\rho(r_\perp,z)=4\sum_{i>0} n_i[(|f_i^+|^2+|f_i^-|^2)+(|g_i^+|^2+|g_i^-|^2)]t_i\ , \quad (12c)$$

$$\rho_c(r_\perp,z)=2\sum_{i>0} n_i[(|f_i^+|^2+|f_i^-|^2)+(|g_i^+|^2+|g_i^-|^2)](\tfrac{1}{2}-t_i)\ . \quad (12d)$$

The nucleons occupy degenerate $\pm m$ orbits, leading to intrinsic states for even-even nuclei which are symmetric under time reversal.

For the case of spherical symmetry the large and small components $f_i(r)$ and $g_i(r)$ of the Dirac spinor ψ_i can be expanded separately in terms of the radial functions $R_{nl_i}(r)$ of a spherical harmonic-oscillator potential $V_{\text{osc}}(r)=\frac{1}{2}M\omega^2 r^2$ with the oscillator frequency $\hbar\omega_0$ and oscillator length

$$b_0=\sqrt{\hbar/M\omega_0}\ ,$$

$$f_i(r)=\sum_{n=1}^{n_{\max}} f_n^i R_{nl_i}(r)\ , \quad (13a)$$

$$g_i(r)=\sum_{\bar{n}=1}^{\bar{n}_{\max}} g_{\bar{n}}^i R_{\bar{n}\bar{l}_i}(r)\ . \quad (13b)$$

For deformed nuclei with axial symmetry we expand the spinors $f_i^\pm$ and $g_i^\pm$ in terms of a deformed harmonic-oscillator potential basis, taking volume conservation into account. The frequencies $\hbar\omega_\perp$ and $\hbar\omega_z$ can be expressed in terms of a deformation parameter β_0 as

$$\hbar\omega_z = \hbar\omega_0 \exp(-\sqrt{5/4\pi}\beta_0) , \tag{14a}$$

$$\hbar\omega_\perp = \hbar\omega_0 \exp(\tfrac{1}{2}\sqrt{5/4\pi}\beta_0) . \tag{14b}$$

We solve the set of Eqs. (11) and (12) self-consistently in the cylindrical coordinates with Ω (the projection of the total angular momentum on the symmetry axis) as a good quantum number. In numerical calculation the wave functions are expanded in a deformed harmonic oscillator potential basis with the maximum oscillator shells $N_{\max}=8$ for nucleons and $N_{\max}=10$ for the bosons. From these converged solutions we obtain the various physical quantities for the deformed nuclei. The quadrupole moment Q and deformation parameter β of the system are calculated from the formulas

$$Q_{n,p} \langle \sum_i 2r_i^2 P_2(\cos\theta_i) \rangle_{n,p} \tag{15a}$$

and

$$Q = Q_n + Q_p = \sqrt{16\pi/5}(3/4\pi A R^2 \beta) , \tag{15b}$$

where $R = 1.2A^{1/3}$

$$\beta_p = \sqrt{5\pi}\frac{Q_p}{3ZR^2} , \tag{15c}$$

$$\beta_n = \sqrt{5\pi}\frac{Q_n}{3NR^2} . \tag{15d}$$

The charge radius is given by

$$r_c = \sqrt{r_p^2 + 0.64} , \tag{16}$$

while the rms matter radius $r_{\rm rms}$ is defined as

$$\langle r_{\rm rms}^2 \rangle = \frac{1}{A}\int \rho(r_\perp, z) r^2 d\tau . \tag{17}$$

Analogous definitions of proton and neutron radii are

$$\langle r_p^2 \rangle = \frac{1}{Z}\int \rho_p(r_\perp, z) r_p^2 d\tau_p$$

and

$$\langle r_n^2 \rangle = \frac{1}{N}\int \rho_n(r_\perp, z) r_n^2 d\tau_n ,$$

respectively.

The energy of the system is given by the expression

$$E = \int d^3r \mathcal{H}(r)$$

$$= E_{\rm part} + E_\sigma + E_\omega + E_\rho + E_C . \tag{18}$$

To Eq. (18) we have to add the pairing energy and energy correction due to center-of-mass motion [5,24]. Thus

$$E_{\rm total} = E_{\rm part} + E_\sigma + E_\omega + E_\rho + E_C + E_{\rm pair} + E_{\rm c.m.} , \tag{19}$$

where

$$E_{\rm part} = \sum_i v_i^2 \int d^3r \psi_i^\dagger [-\vec{\alpha}\cdot\vec{\nabla} - \vec{\alpha}\cdot\vec{V}$$

$$+ \beta M^* + V(r_\perp, z)]\psi_i , \tag{20a}$$

$$E_\sigma = \int d^3r [\tfrac{1}{2}(\nabla\sigma)^2 + U(\sigma)] , \tag{20b}$$

$$E_\omega = -\int d^3r [\tfrac{1}{2}(\nabla V_0)^2 + \tfrac{1}{2}m_\omega^2 V_0^2] , \tag{20c}$$

$$E_\rho = -\int d^3r [\tfrac{1}{2}(\nabla\rho_0)^2 + \tfrac{1}{2}m_\rho^2 \rho_0^2] , \tag{20d}$$

$$E_C = -\int d^3r \tfrac{1}{2}[(\nabla A_0)^2] , \tag{20e}$$

$$E_{\rm pair} = -G\left[\sum_{i>0} u_i v_i\right]^2 , \tag{20f}$$

$$E_{\rm c.m.} = -\tfrac{3}{4}41A^{-1/3} . \tag{20g}$$

In Eq. (19) $E_{\rm part}$ is the energy of the particles moving in the field created by the mesons. E_σ, E_ω, E_ρ, and E_C are the energies of the meson fields and the Coulomb field. $E_{\rm pair}$ is the pairing energy with the pairing force strength G and the occupation and unoccupation probabilities v_i^2 and $u_i^2 = 1 - v_i^2$. $E_{\rm c.m.}$ is the center-of-mass correction and here we have approximated it by its value in a nonrelativistic harmonic-oscillator potential [5,9,24]. We follow the procedure of Gambhir, Ring, and Thimet [5] to evaluate the pairing energy; the pairing gaps Δ_p and Δ_n are taken from the experimental even-odd mass difference [14]. The chemical potentials λ_p and λ_n are determined by solving the number equations:

$$\mathcal{N} = \sum_i n_i = \sum_i v_i^2$$

$$= \frac{1}{2}\sum_i \left[1 - \frac{E_i - \lambda}{\sqrt{(E_i-\lambda)^2 + \Delta^2}}\right] . \tag{21}$$

The summation in Eq. (21) and in Eq. (23) (below) extends up to $2\hbar\omega_0(2\times 41A^{-1/3})$ above the Hartree-Fock Fermi energy [5]

$$u_i^2 = 1 - v_i^2 , \tag{22}$$

$$E_{\rm pair} = -\Delta \sum_{i>0} u_i v_i . \tag{23}$$

We have solved the equations given in this section iteratively following the numerical procedure of Gambhir, Ring, and Thimet. In Sec. III we present the results of calculation of various physical quantities for even mass Ca, Ti, Cr, Fe, Ni, and Zn nuclei.

III. PROPERTIES OF MESONS AND CHOICE OF PARAMETERS

The field corresponding to the isoscalar-scalar σ meson, which is a very broad two-pion resonance state (s wave), provides strong scalar attraction at long distance (>0.4 fm). The isoscalar vector meson ω, which is a 3π-resonance state, gives the strong repulsion at short distance. Similarly, the field due to the isovector vector ρ meson (p-state 2π resonance) is important for proton-neutron asymmetric systems, because it couples to the isospin current. Here we have considered the scalar (nonlinear) σ field and the vector coupling of ω and ρ. The tensor couplings of the vector mesons ω and ρ (i.e., $\bar{\psi}\sigma_{\mu\nu}\psi\Omega^{\mu\nu}$ and $\bar{\psi}\vec{\tau}\cdot\sigma_{\mu\nu}\psi\vec{R}\mu\nu$) do not contribute for even-even nuclei in the RMF approximation used, because of

time-reversal symmetry and parity (see appendix). The fields corresponding to π mesons are not considered because these do not contribute in this RMF approximation for the Hartree states having good parity.

In this paper, we have presented the results, taking the parameter set NL1 of Table 1. In Table 1 we give the parameters for the linear set L1 and the nonlinear sets NL1 and NL2 (Refs. [37,4,33]). Some results of calculations for finite nuclei using the parameter sets L1, NL1, and NL2 are given in Table II. The set L1 consistently yields overbinding and hence results in smaller values of rms radii. Therefore, we do not present in detail the results of this parameter set. However, to illustrate this point explicitly, results for specific cases only (^{48}Ca, ^{48}Ti, ^{52}Cr, ^{56}Fe, ^{56}Ni, ^{60}Ni, ^{62}Ni, ^{64}Ni, ^{66}Ni, ^{68}Ni and ^{64}Zn) using the parameter set L1 are presented.

Further, inspection of Table II reveals that the results for the set NL2 give rather large underbinding and those for the set NL1 agree much better with experimental binding energies. The set NL1 also gives a more reasonable nuclear compressibility (Table I).

To see the sensitivity of the results to the ρ-meson coupling strength, we have presented in Table III the results of some observables of our RMF calculations with different ρ-meson coupling constants (g_ρ varying from 4.9755 to 4.0). The change of nuclear radii and quadrupole deformations (β) with the coupling strength of the ρ meson is negligible. The sensitivity to the total binding energy is about 1%, when g_ρ changes from 4.9755 to 4.0. Thus the results are not very sensitive to a reasonable variation in the ρ-meson coupling strength [39].

Recently Toki *et al.* [40] have studied the properties of infinite nuclear matter and spherical nuclei using a linear sigma version relativistic Hartree theory. Their aim is not to reproduce the experimental observables of nuclei around the stability line. Rather, they intend to study the qualitative aspects of the effect of ρ-meson field on the properties of nuclei far from stability line. In their calculations, they found that the neutron and proton radii are insensitive to the ρ-meson coupling strength, but the neutron-drip line shows some sensitivity to the ρ-meson coupling strength without changing the other general properties significantly. It is to be pointed out that Toki *et al.* varied g_ρ over a very large parameter range to study the sensitivity to ρ-meson coupling.

The present paper has a different aim, namely, to study the equilibrium properties of finite nuclei using relativistic mean field theory having nonlinear σ terms. The nonlinear terms are given by the parameters g_2 and g_3 of Eq. (2). The mass of the ρ meson m_ρ is fixed to the corresponding meson mass ($m_\rho = 763$ MeV) in an OBEP [4,41]. The other parameters of the nonlinear set NL1 are least-squares fitted with respect to total binding energies, diffraction radii and surface thickness in eight spherical nuclei [4], namely, ^{16}O, ^{40}Ca, ^{48}Ca, ^{58}Ni, ^{90}Zr, ^{116}Sn, and ^{208}Pb. Results for other nuclei are obtained as predictions of the model. The values of g_s, g_ω, g_ρ, g_2, and g_3 and masses of σ and ω mesons (m_σ and m_ρ) thus obtained constitute the nonlinear parameter set NL1 of Table I. (Note that the definition of g_ρ here is different from that of Refs. [3] and [4] by a factor of 2.) The effective mass at the center of the nucleus and also other properties of NL1 are given in Table I.

The nonlinear parameter set NL1 of Table I gives the

TABLE I. Various parameter sets for the Lagrangian [Eq. (1)] and the corresponding derived quantities. The masses, compressibility K, and symmetry energy coefficient $a_{\rm sym}$ are in MeV, saturation density ρ_0 is in fm^{-3}, and g_2 is in fm^{-1}. The other coupling constants are dimensionless. The quantities in the last five lines are obtained from the model.

Parameter	L1[a]	NL1[b]	NL2[c]	Empirical Value
M	938.0	938.0	938.0	938.0
m_σ	550.0	492.25	504.89	...
m_ω	783.0	795.359	780.0	783±5
m_ρ	...	763.0	763.0	773±77
g_s	10.3	10.138	9.111	
g_ω	12.6	13.285	11.493	
g_ρ	...	4.9755	5.507	
g_2	0.0	−12.172	−2.304	
g_3	0.0	−36.265	13.783	
$\frac{M^*}{M}$	0.53	0.57	0.67	
K	626.3	211.7	399.2	210±30[d]
$a_{\rm sym}$		43.6		
ρ_0		0.1542		0.17[e]
BE/A	(nucl. matter)	16.43 MeV		15.68[e] MeV

[a]Reference [37].
[b]Reference [4].
[c]Reference [38].
[d]Reference [43].
[e]Reference [48].

TABLE II. Some representative observables using various parameter sets. The total binding energy BE is in MeV and rms charge radius r_c is fm.

Nuclei	Set	BE (calc.)	BE (expt.)	r_c (calc.)	r_c (expt.)
^{48}Ca	L1	436.470	415.993	3.240	3.481
	NL1	412.171		3.513	
	NL2	404.508		3.499	
^{48}Ti	L1	443.153	418.702	3.313	3.570
	NL1	414.679		3.577	
	NL2	410.798		3.564	
^{52}Cr	L1	491.890	456.350	3.366	3.670
	NL1	453.674		3.632	
	NL2	445.539		3.692	
^{56}Fe	L1	531.450	492.260	3.448	3.743
	NL1	489.362		3.677	
	NL2	481.984		3.776	
^{56}Ni	L1	536.398	483.993	3.460	
	NL1	483.448		3.677	
	NL2	473.402		3.784	
^{60}Ni	L1	569.362	526.848	3.515	3.818
	NL1	522.888		3.737	
	NL2	515.897		3.862	
^{62}Ni	L1	583.703	545.265	3.534	3.847
	NL1	540.864		3.774	
	NL2	534.642		3.870	
^{64}Ni	L1	599.078	561.760	3.553	3.866
	NL1	558.349		3.811	
	NL2	550.197		3.865	
^{66}Ni	L1	611.792	576.834	3.573	3.920
	NL1	576.115		3.848	
	NL2	571.204		3.871	
^{68}Ni	L1	623.447	590.431	3.584	
	NL1	589.833		3.877	
	NL2	578.678		3.896	
^{64}Zn	L1	599.669	559.100	3.618	3.933
	NL1	555.331		3.909	
	NL2	548.583		3.929	

TABLE III. Variation of observables of ^{68}Ni with g_ρ. The experimental binding energy of ^{56}Ni is 590.431 MeV. The binding energy BE is in MeV, rms radii (neutron r_n, proton r_p, matter $r_{\rm rms}$, and charge radius r_c) are in fm, β_n, β_p, and β are the deformation parameter of neutron, proton, and total deformation, respectively.

g_ρ	BE	r_n	r_p	$r_{\rm rms}$	r_c	β_n	β_p	β
4.9755	589.833	4.072	3.793	3.960	3.877	−0.000 11	−0.000 00	−0.000 07
4.75	591.395	4.067	3.795	3.957	3.878	−0.000 10	−0.000 00	−0.000 06
4.7	591.788	4.066	3.795	3.957	3.878	−0.000 07	−0.000 03	−0.000 03
4.6	591.102	4.064	3.796	3.956	3.879	−0.000 09	−0.000 01	−0.000 05
4.5	593.390	4.061	3.796	3.954	3.880	−0.000 06	0.000 04	−0.000 02
4.4	594.264	4.059	3.797	3.953	3.880	−0.000 05	0.000 05	−0.000 01
4.3	595.790	4.057	3.798	3.952	3.881	−0.000 05	0.000 04	−0.000 01
4.2	596.874	4.055	3.799	3.951	3.882	−0.000 04	0.000 05	−0.000 01
4.1	596.852	4.052	3.799	3.950	3.883	−0.000 04	0.000 05	0.000 00
4.0	596.978	4.050	3.800	3.949	3.884	−0.000 03	0.000 05	0.000 00

nuclear matter binding energy per particle BE/A = 16.43 MeV and the saturation density $\rho_0 = 0.1542$ fm^{-3}. The symmetry energy coefficient a_{sym} comes out [4] to be 43.6 MeV, which is a bit too high compared to $a_{sym} \approx 35$ MeV as assumed by other authors [3,42]. The compressibility K using NL1 parameter set is 211.7 MeV, whereas the empirical value [43] is 210±30 MeV.

IV. RESULTS

In this section we present the results of our calculation for a number of isotopes of Ca, Ti, Cr, Fe, Ni, and Zn. Some of the results of our calculation are given in Tables IV–VIII along with some known experimental quantities.

A. Binding energies and neutron-drip lines

Empirically it is known (see, e.g., Ref. [14], Chap. 2) that some of the most stable nuclei occur in the $A \approx 56$ region, where the BE/A (binding energy per nucleon) curve shows a peak. In Fig. 1 we have plotted the binding energy per nucleon obtained in our RMF calculation against neutron number for the even-even isotopes with $Z = 20-30$.

The agreement of our calculation with the experimentally known binding energies is remarkably good (Tables IV and V). For example, we get for ^{40}Ca BE/A of 8.515 MeV (experimentally 8.551 MeV); for ^{42}Ca our calculation gives BE/A of 8.598 MeV (experimentally 8.617 MeV). On the whole the agreement of the calculated binding energies with the experimental ones is significantly better than the prediction of mass formulas or predictions of Skyrme interaction calculations. From Fig. 1 we see that the largest BE/A for Ca isotopes occurs near $N = 26$. The point of maximum BE/A shifts to large neutron numbers for higher Z isotopes. The point of maximum binding energy clusters around $N = 28$ for Z values up to Ni. For Zn the maximum binding energy per particles occurs at $N = 40$. Our calculation for neutron-rich nuclei should be more reliable than the mass formula extrapolations, because we take into account the coupling with ρ meson and other mesons at a microscopic level. We have calculated the binding energies, rms radii, etc., for nuclei up to the neutron-drip line. In Fig. 1 the neutron-drip line is indicated as dashed line. In Table VIII we have compared our RMF calculation results for the neutron-drip lines in even $Z = 20-30$ with those predicted from mass formulas. In general we find a larger number of stable isotopes (before reaching the drip line) than predicted by the mass formulas.

B. Spherical shell effects

One of the advantages of the relativistic mean field description of nuclei is that all the relevant properties of

TABLE IV. Comparison between calculated results of binding energy per particle (BE/A), charge radius r_c with experimental results and total deformation parameter β with Moeller and Nix prediction[a] for Ca, Ti, and Cr. BE/A is in MeV and radii are in fermi.

Nuclei	N	BE/A (calc.)	BE/A (expt.)[b]	r_c (calc.)	r_c (expt.)	$\beta_{\text{This work}}$	$\beta^{a}_{\text{Moeller-Nix}}$
^{20}Ca	16	7.843	7.816			−0.006 45	−0.148 420
	18	8.247	8.240			−0.005 47	−0.024 210
	20	8.515	8.551	3.508	3.480[c]	0.001 21	0.003 158
	22	8.598	8.617	3.507	3.510[c]	0.007 57	0.003 158
	24	8.605	8.658	3.501	3.520[c]	0.012 76	0.003 158
	26	8.615	8.669	3.503	3.501[c]	0.016 40	0.010 526
	28	8.587	8.656	3.513	3.481[c]	0.006 25	0.003 158
	30	8.550	8.479	3.515	3.480[d]	0.002 74	0.010 526
^{22}Ti	20	8.307	8.260			0.000 37	0.003 158
	22	8.460	8.534			0.007 22	0.017 895
	24	8.541	8.656	3.586	3.590[e]	0.032 96	0.024 211
	26	8.639	8.723	3.578	3.590[e]	0.067 59	0.038 947
	28	8.695	8.756	3.577	3.570[e]	0.005 24	0.017 895
	30	8.615	8.692			0.028 29	0.046 316
^{24}Cr	20	7.911	7.950			0.000 39	0.003 158
	22	8.206	8.304			0.205 85	0.031 579
	24	8.512	8.572			0.272 72	0.223 160
	26	8.654	8.701	3.650	3.680[e]	0.236 85	0.145 263
	28	8.725	8.776	3.632	3.670[e]	0.145 00	0.024 210
	30	8.711	8.778	3.649	3.710[e]	0.183 69	0.137 895
	32	8.638	8.636			0.193 82	0.166 316

[a]Reference [33].
[b]Refernece [10].
[c]Reference [32].
[d]Reference [31].
[e]Reference [30].

TABLE V. Same as Table IV for Fe, Ni, and Zn.

Nuclei	N	BE/A (calc.)	BE/A (expt.)[a]	r_c (calc.)	r_c (expt.)	$\beta_{\text{This work}}$	$\beta^{b}_{\text{Moeller-Nix}}$
$_{26}$Fe	24	8.309	8.354			0.245 52	0.137 895
	26	8.541	8.610			0.217 49	0.116 842
	28	8.713	8.736	3.649	3.700[c]	0.049 95	0.024 211
	30	8.739	8.790	3.677	3.743[c]	0.158 76	0.124 211
	32	8.710	8.792	3.725	3.780[c]	0.190 68	0.173 684
	34	8.680	8.756			0.175 75	0.194 737
	36	8.644	8.693			0.132 71	0.158 947
$_{28}$Ni	26	8.363	8.392			0.045 15	0.024 211
	28	8.633	8.642			0.013 84	0.010 526
	30	8.712	8.732	3.695	3.781[c]	0.018 31	0.031 579
	32	8.715	8.781	3.737	3.818[c]	0.081 64	0.060 000
	34	8.724	8.795	3.774	3.847[c]	0.064 94	0.074 737
	36	8.724	8.778	3.811	3.866[c]	0.047 25	−0.088 421
	38	8.729	8.740	3.848	3.920[d]	−0.006 59	−0.038 947
	40	8.674	8.683			−0.000 07	−0.003 158
$_{30}$Zn	26	8.072	8.119			0.171 83	0.151 579
	28	8.385	8.394			0.009 62	0.031 579
	30	8.526	8.583			0.181 11	0.158 950
	32	8.615	8.679			0.205 56	0.180 000
	34	8.677	8.736	3.909	3.933[c]	0.202 92	0.180 000
	36	8.679	8.760	3.926	3.954[c]	0.171 74	0.180 000
	38	8.686	8.756	3.941	3.971[c]	0.119 55	0.145 260
	40	8.699	8.730	3.953	3.989[c]	0.002 89	0.202 110
	42	8.645	8.692			0.022 27	0.145 260
	44	8.600	8.642			0.157 90	0.151 579
	46	8.531	8.582			0.188 05	0.145 263

[a]Reference [10].
[b]Reference [33].
[c]Reference [15].
[d]Reference [31].

nuclei can be obtained starting with the interacting nucleons and mesons. It turns out that the all-important shell effect (including spin-orbit interaction) arises from the solutions of self-consistent RMF equations of interacting nucleons and mesons without any *ad hoc* assumptions. The spherical shapes for $N=20$, 28, 40, and 50 are evident in the β_n value plots in Fig. 2 for Cr and Ni nuclei. This tendency for spherical shape at $N=20$, 28, 40, and 50 is present for Ca, Ti, Fe, and Zn nuclei also. The Hartree-Fock orbitals show large gaps for neutron numbers 20, 28, and 50, corresponding to the well-known shell gaps for these magic numbers. $N=40$ nuclei do not have large energy gaps but have spherical shapes corresponding to $2p_{1/2}$ subshell closure. These trends are

TABLE VI. Calculated result of r_n, r_p, r_{rms}, β_n, β_p, and the total deformation β of the ^{22}Ti nuclei. Radii are in fermi.

Nuclei	N	r_n	r_p	r_{rms}	β_n	β_p	β
$_{22}$Ti	20	3.381	3.506	3.447	0.000 46	0.000 37	0.000 41
	22	3.452	3.497	3.475	0.007 15	0.007 22	0.007 19
	24	3.526	3.496	3.511	0.037 46	0.032 96	0.035 31
	26	3.578	3.487	3.537	0.077 73	0.067 59	0.073 08
	28	3.642	3.486	3.574	0.005 68	0.005 24	0.005 49
	30	3.722	3.495	3.628	0.035 17	0.028 29	0.032 26
	32	3.808	3.511	3.690	0.000 18	0.000 15	0.000 17
	34	3.905	3.549	3.769	0.042 56	0.031 94	0.038 34
	36	3.989	3.587	2.841	0.027 36	0.018 98	0.024 18
	38	4.066	3.627	3.911	−0.011 03	−0.005 74	−0.009 09
	40	4.139	3.663	3.976	−0.002 20	−0.001 40	−0.001 91
	42	4.194	3.681	4.025	0.049 98	0.017 65	0.038 87
	44	4.267	3.708	4.089	0.126 80	0.078 28	0.110 63

TABLE VII. Same as Table VI for Zn.

Nuclei	N	r_n	r_p	$r_{\rm rms}$	β_n	β_p	β
$_{30}$Zn	26	3.560	3.746	3.661	0.161 84	0.180 48	0.171 83
	28	3.564	3.692	3.630	0.007 90	0.011 23	0.009 62
	30	3.715	3.766	3.741	0.175 01	0.187 21	0.181 11
	32	3.812	3.799	3.805	0.203 70	0.207 56	0.205 56
	34	3.894	3.826	3.862	0.201 64	0.204 36	0.202 92
	36	3.964	3.843	3.909	0.166 84	0.177 62	0.171 74
	38	4.025	3.859	3.953	0.110 67	0.130 80	0.119 55
	40	4.079	3.871	3.991	0.004 61	0.000 60	0.002 89
	42	4.143	3.893	4.040	0.020 11	0.025 28	0.022 27
	44	4.211	3.920	4.095	0.153 40	0.164 52	0.157 90
	46	4.263	3.939	4.138	0.185 75	0.191 58	0.188 05
	48	4.309	3.949	4.174	0.162 05	0.169 93	0.165 08
	50	4.360	3.957	4.213	0.040 58	0.044 92	0.042 21
	52	4.390	3.949	4.234	0.100 56	0.093 14	0.097 85
	54	4.466	3.976	4.297	0.183 92	0.150 67	0.172 04
	56	4.535	3.998	4.355	0.200 46	0.160 55	0.186 54
	58	4.600	4.021	4.411	0.201 04	0.154 30	0.185 11
	60	4.658	4.043	4.463	0.189 18	0.146 98	0.175 11
	62	4.751	4.105	4.550	0.194 58	0.174 92	0.188 17

consistent with experimental systematics and also with the results of Hartree-Fock calculations using Skyrme interactions [27]. For Ca and Ti isotopes we find a sharp dip in the neutron quadrupole deformation (β_n) at $N=32$ (Fig. 2 and Tables VI,VII) indicating a preference for spherical shape for ^{52}Ca and ^{54}Ti, associated with the $p_{3/2}$ subshell closure for $N=32$ [11]. For Cr, Fe, Ni, and Zn no such dip in quadrupole deformation is found for $N=32$.

C. Systematics of quadrupole deformation

Apart from the magic shell closures at $N=20$, 28, 50 and the subshell closures at $N=32$ and 40 discussed in Sec. IVB, the majority of nuclei studied in the present work show a tendency for quadrupole deformation. The neutron and proton quadrupole deformations β_n and β_p are plotted as a function of neutron number for Ca, Cr, Fe, and Ni nuclei in Figs. 2 and Tables VI,VII. Besides the dips in deformation near shell closures (or subshell closures), one sees some spectacular peaks in deformation for some specific neutron numbers ($N\approx 24, 32, 46$).

On the whole Ca isotopes are the least deformed and Cr isotopes are the most deformed of nuclei studied in this work. In ^{56}Ni we find the prolate minimum ($\beta\approx 0.014$) to be the lowest in energy. The spherical minimum, with $f_{7/2}$ proton and neutron shell closures, is found to be about 1 MeV above the prolate minimum. It may be remarked that in conventional Hartree-Fock calculation [26], ^{56}Ni is also found to be a deformed nucleus.

D. Systematics of charge and matter radii

Recently there has been speculation about neutron halo in neutron-rich light nuclei [13]. Actually the nuclei considered by Myers [13] are Li and Be, with considerably smaller charge numbers than the nuclei we are considering here. Even then it is worth investigating the systematics of neutron and proton radii for possible halo effects. From Figs. 3(a), 3(c) and Tables VI,VII we find that the neutron rms radii and the matter rms radii increase considerably as the neutron number is increased (about 30% increase in these radii as neutron number increases from 20 to 60). While this increase is substantial and implies the presence of more and more neutrons near the surface, the increase is not large enough for neutron-halo-like effects. In contrast to the neutron and matter rms radii, for the proton rms radii [Fig. 3(b) and Tables VI,VII] the increase with neutron number is more gradual. In Figs. 3(a)–3(c) we notice a tendency for decrease of

TABLE VIII. Comparison with mass formula results for the neutron-drip line with this calculation.[a]

Nuclei	Expt.	Comay-Kelson	Techibana *et al.*	Masson-Janeke	Moeller *et al.*	Moeller-Nix	This work
$_{20}$Ca	32<	38	38	38	38	38	42
$_{22}$Ti	32<	42	42	42	40	40	44
$_{24}$Cr	34<	46	47	46	43	43	50
$_{26}$Fe	37<	51	51	51	51	51	50
$_{28}$Ni	41<	55	55	55	54	54	60
$_{30}$Zn	50<	58	59	58	56	56	62

[a]Reference [10].

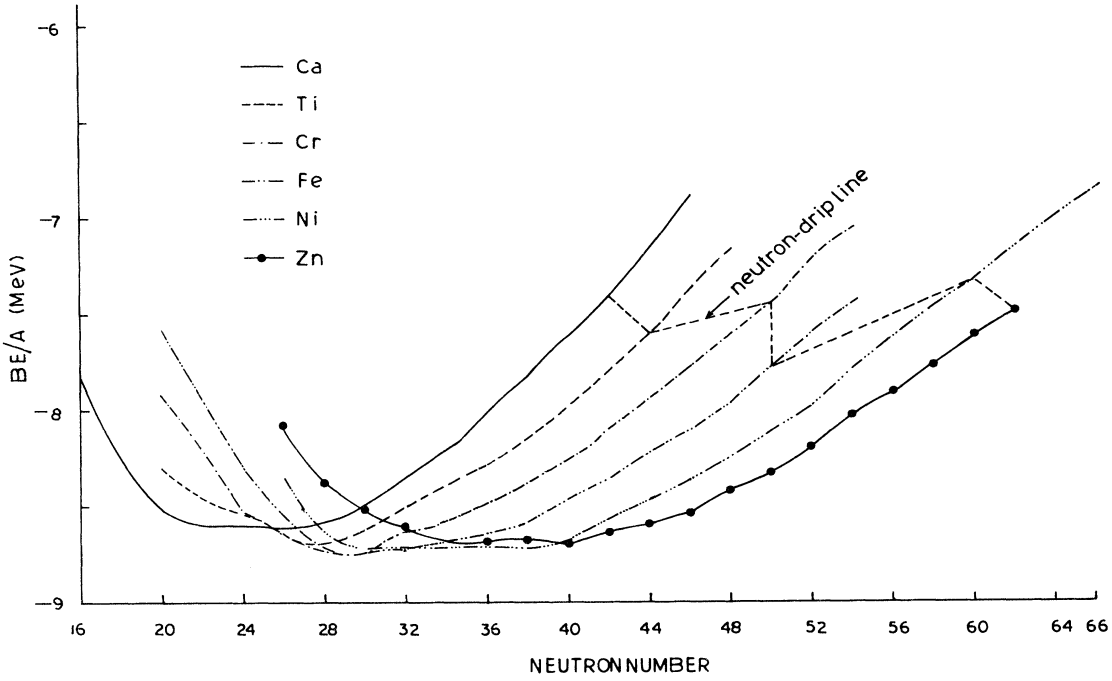

FIG. 1. Plot of binding energy per particle (BE/A) vs neutron number for Ca, Ti, Cr, Fe, Ni, and Zn nuclei. The dashed line at the right indicates neutron-drip line.

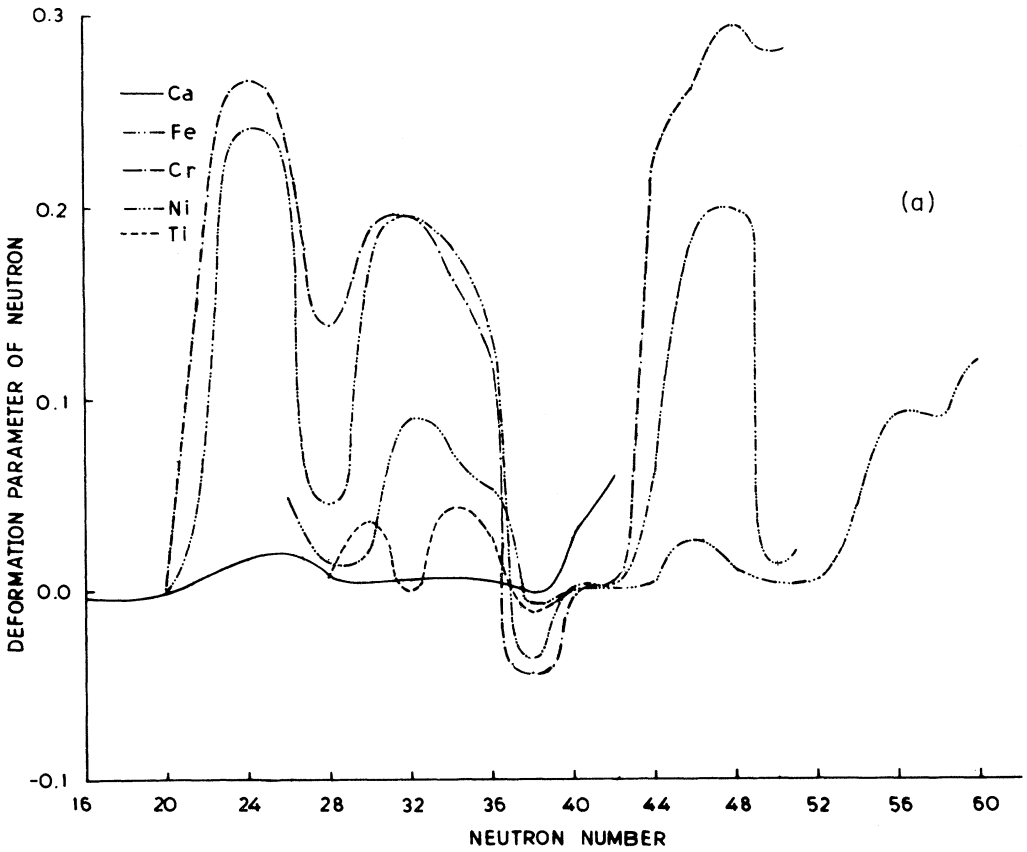

FIG. 2. (a) Plot of deformation parameter of neutron β_n vs neutron number for Ca, Cr, Fe, Ni, and Ti. (b) Plot of deformation parameter of proton β_p vs neutron number.

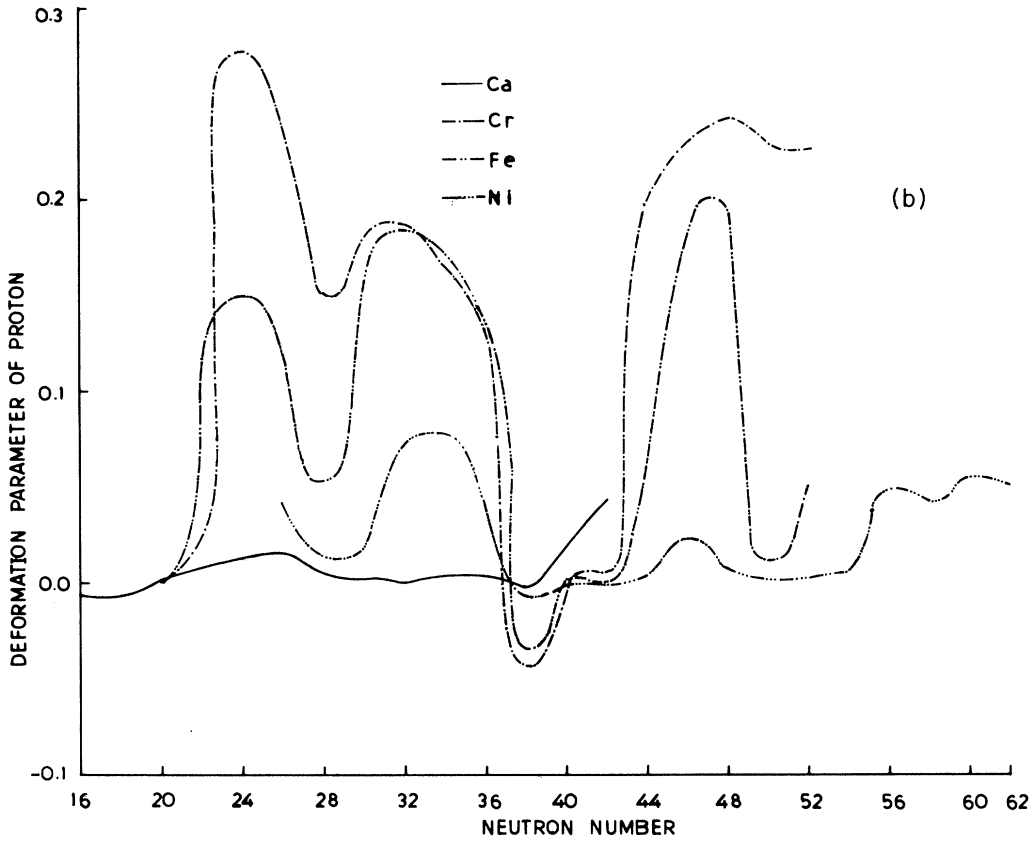

FIG. 2. (*Continued*).

the radii near the spherical neutron shell closures $N=28$ and 50. This is specially so for the higher Z nuclei like Ni and Zn. The neutron-drip line is beyond $N=56$ for Ni and Zn. For these two isotopes the rate of increase in radii slows down near $N=56$. Such isotope effect near $N=56$ is known [35] for nuclei like Mo.

E. Spin-orbit splitting

In RMF calculations, the spin-orbit force comes out automatically when the Dirac equation is solved. Applying the Foldy-Wouthuysen reduction of the single-particle Dirac equation [Eq. 4(a)] for nonrelativistic nucleons moving in the potential generated by the scalar and vector fields allows one to identify the effective single-particle spin-orbit splitting [3,44] as

$$V_{\text{s.o.}}(r)=\frac{1}{2M^2r}\left[g_\omega\frac{dV_0(r)}{dr}+g_s\frac{d\sigma(r)}{dr}\right]\mathbf{l}\cdot\mathbf{s}$$
$$=-\alpha(r)\mathbf{l}\cdot\mathbf{s}\ .$$

Gambhir, Ring, and Thimet [4] studied the single-particle spectra of ^{16}O, ^{90}Zr, and ^{208}Pb as typically representative of spherical nuclei. For ^{16}O they found that the single-particle spectra for neutrons and protons are in reasonable agreement with experiment and are also close to those of Skyrme-II calculations. In particular, the gap at the Fermi surface between the last occupied and the first unoccupied levels is well reproduced for both neutrons and protons. Similarly, the NL1 is able to well reproduce the single-particle spectra of other nuclei as well.

Using NL1 we have calculated the single-particle spectra of ^{40}Ca and we get the spin-orbit splitting as 6.8 and 4.8 MeV for 0*d* and 0*p* orbits, respectively, whereas the experimentally observed values [45] are 8.0 and 4.7 MeV for these orbits, respectively. On the whole the nonlinear σ model (NL1) used here gives a proper description of the spin-orbit splitting in finite nuclei.

V. DISCUSSION

The relativistic mean field theory provides a microscopic model for the gross properties of nuclei. In this work we have studied the gross properties of about 100 even-even nuclei with $Z=20-30$ using the deformed relativistic mean field model of Walecka with the nonlinear corrections of Boguta and Bodmer for the σ meson. Good agreement is obtained for the binding energies and rms radii between our calculation and some experimentally known nuclei. The quadrupole deformation parameters calculated in the present work show overall agreement with those in the calculation of Moeller and Nix.

We have done the relativistic mean field calculations for the neutron-rich species of these isotopes till the neutron-drip line. The results for the neutron-drip line conform overall with those of extrapolation of various mass formulas, although our calculation predicts a few

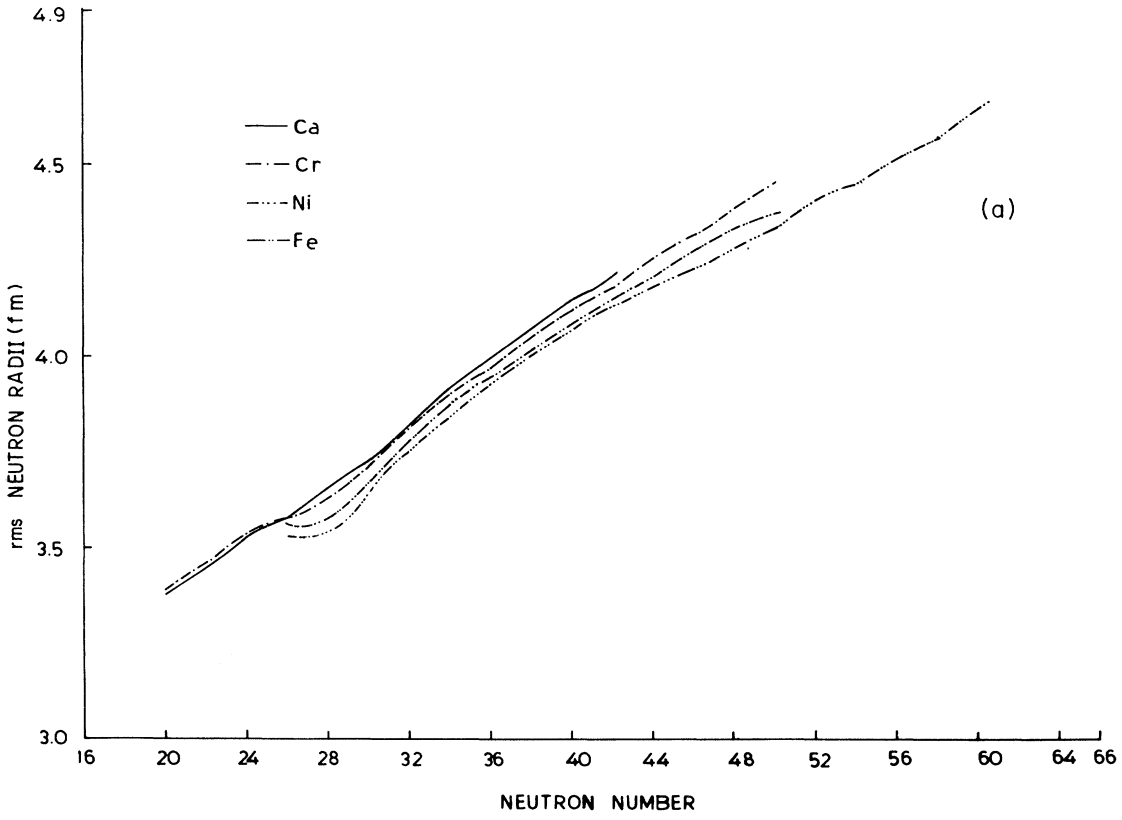

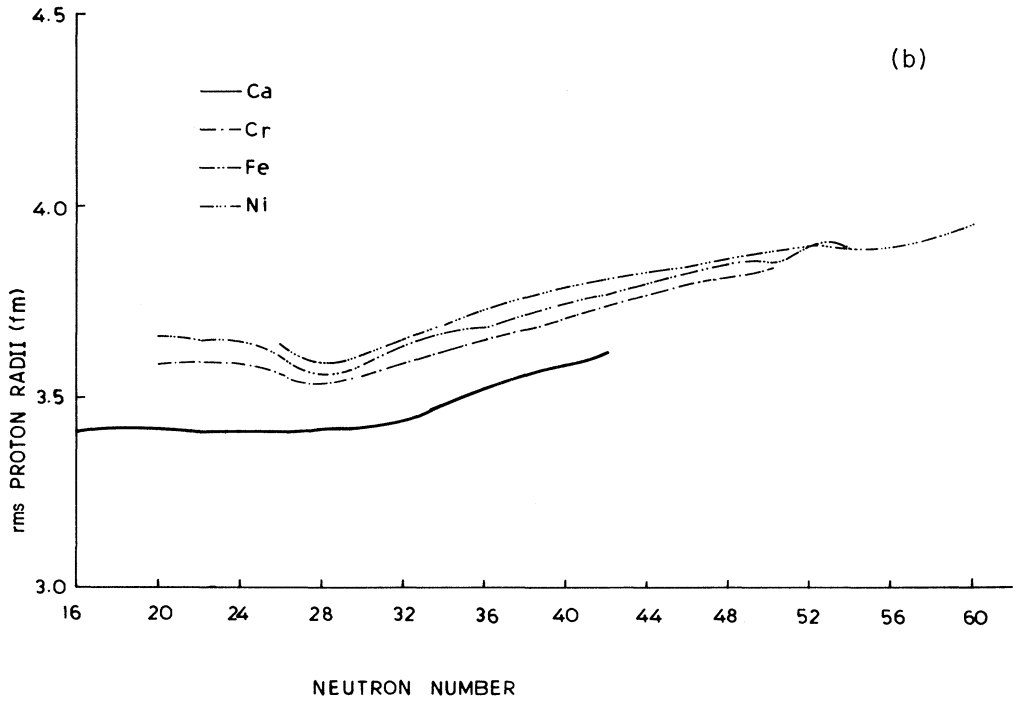

FIG. 3. (a) Plot of neutron radius r_n vs neutron number. (b) Plot of proton radius r_p vs neutron number. (c) Plot of matter radius r_{rms} vs neutron number

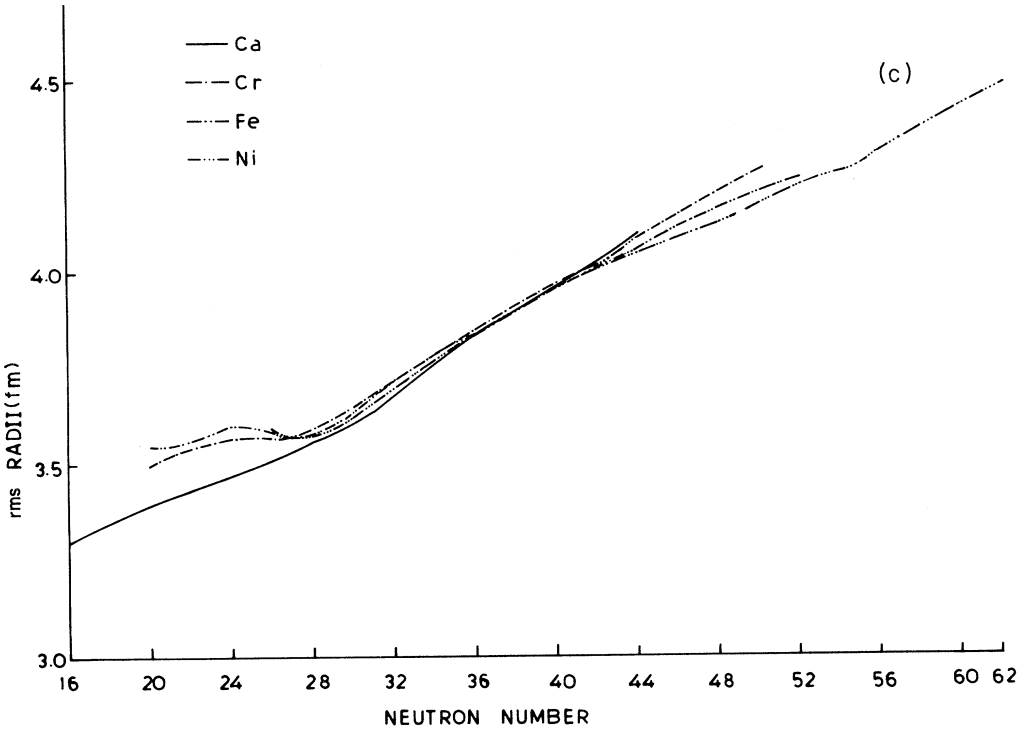

FIG. 3. (*Continued*).

more nuclei than the mass formula extrapolations. The results indicate that there remain a considerable number of neutron-rich nuclei still to be discovered in this mass region and such nuclei should be looked for in experiments. Of course these nuclei are stable against decay by neutron emission, but would in general be subject to β decays.

The results of our calculation for rms radii show good agreement with known experimental results. The rms radii and the quadrupole deformation parameters, calculated in the RMF formulation, show characteristic shell closure effects. The quadrupole deformation parameter has maxima for neutron numbers 24 and 46. For $N=32$, the quadrupole deformation shows minima for Ca and Ti corresponding to spherical subshell closure, while for the other isotopes Cr, Fe, Ni, and Zn, we see maxima in deformation parameter. In general Cr nuclei are the most deformed of these nuclei. Also Fe and Zn nuclei have substantial deformation.

Thus the RMF, while giving excellent results for the experimentally known binding energies and radii in the $Z=20-30$ region, gives valuable insight into the shape and isotope effects in these nuclei and the neutron-drip line.

Many of the nuclei studied in this work are deformed (Tables IV–VII). In principle, to get the spectra for these nuclei, states of good angular momenta should be obtained from the deformed intrinsic states using the angular momentum projection operator [46]. Here we deal with nucleon and meson fields simultaneously and hence one has to project angular momentum for all these fields in a relativistic formalism. However, in this work we are concerned with binding energies, nuclear deformations, and the average properties of the intrinsic states and not the spectroscopy of the bands in these nuclei. Hence we have not considered angular momentum projection in this work. Angular momentum projection for relativistic mean field models remains an interesting problem for future investigations.

We thank Professor S. P. Misra, Professor Y. K. Gambhir, Professor M. A. Nagarajan, and Dr. J. A. Sheikh for many stimulating discussions.

APPENDIX: TENSOR COUPLING OF VECTOR MESONS AND SYMMETRIES OF THE MEAN FIELD SOLUTIONS

The tensor coupling of a vector meson (ω or ρ meson) with nucleons involves coupling of the type

$$\bar{\psi}\sigma_{\mu\nu}\psi\Omega^{\mu\nu} . \tag{A1}$$

Here

$$\sigma_{\mu\nu}=\frac{i}{2}(\gamma_\mu\gamma_\nu-\gamma_\nu\gamma_\mu) \tag{A2}$$

and $\Omega^{\mu\nu}$ is the field tensor defined in Eq. (3b) for the vector field V. With

$$\vec{\gamma}=\begin{bmatrix} 0 & \vec{\sigma} \\ -\vec{\sigma} & 0 \end{bmatrix} \tag{A3}$$

and

$$\gamma^0=\begin{bmatrix}1 & 0\\ 0 & -1\end{bmatrix}, \tag{A4}$$

expression (A1) becomes [47]

$$\bar{\psi}(-\vec{\sigma}\cdot\vec{H}+i\gamma_4\vec{\gamma}\cdot\vec{E})\psi\ , \tag{A5}$$

where

$$\vec{H}=\vec{\nabla}\times\vec{V} \tag{A6}$$

is the equivalent of the "magnetic" field and

$$\vec{E}=-\frac{\partial\vec{V}}{\partial t}-\vec{\nabla}V_0 \tag{A7}$$

is the "electric" field of the vector meson. $\vec{\sigma}=\begin{pmatrix}\vec{\sigma} & 0\\ 0 & \vec{\sigma}\end{pmatrix}$ is the relativistic generalization of the nucleon spin.

The expectation value of $\vec{\sigma}$ in expression (A5) for a many-nucleon configuration having time-reversal symmetry (even-even nuclei) vanishes and hence the first term of expression (A5) does not occur in the mean field equations. Similarly the $\langle\gamma_4\vec{\gamma}\rangle$ expectation value vanishes for states having good parity and hence the second term of expression (A5) also does not contribute in the approximation used here. Thus the tensor coupling (A1) does not contribute to the mean field solution of even-even nuclei.

[1] J. D. Walecka, Ann. Phys. (N.Y.) **83**, 491 (1974).
[2] B. D. Serot and J. D. Walecka, Adv. Nucl. Phys. **16**, 1 (1986).
[3] C. J. Horowitz and B. D. Serot, Nucl. Phys. **A368**, 503 (1981).
[4] P. G. Reinhard *et al.* Z. Phys. A **323**, 13 (1986).
[5] Y. K. Gambhir, P. Ring, and A. Thimet, Ann. Phys. (NY) **198**, 132 (1990).
[6] J. Boguta and A. R. Bodmer Nucl. Phys. **A292**, 413 (1977).
[7] C. E. Price and G. E. Walker, Phys. Rev. C **36**, 354 (1987).
[8] J. Zimanyi and S. A. Moszkowski, Phys. Rev. C **42**, 1416 (1990).
[9] J. W. Negele, Phys. Rev. C **1**, 1260 (1970).
[10] A. H. Wapstra, G. Audi, and R. Hoekstra, At. Data Nucl. Data Tables **39**, 281 (1988).
[11] A. Huck *et al.*, Proceedings of the 4th International Conference on Nuclei Far from Stability, Selsingor, Denmark, 1981 (CERN 81-09), Vol. II, p. 378.
[12] Y. Schutz, GANIL (Caen, France) Report No. 89, 1990.
[13] W. D. Myers, Lawrence Berkely Laboratory Report No. LBL-27874.
[14] A. Bohr and B. R. Mottelson, *Nuclear Structure* (Benjamin, New York, 1969), Vol. I.
[15] E. B. Shera *et al.* Phys. Rev. C **14**, 731 (1976).
[16] L. D. Miller, Phys. Rev. C **14**, 706 (1976).
[17] R. J. Furnstahl and C. E. Price, Phys. Rev. C **40**, 1398 (1989); R. J. Furnstahl, C. E. Price, and G. E. Walker, *ibid.* **36**, 2590 (1987).
[18] Y. K. Gambhir and P. Ring, Phys. Lett. B **202**, 5 (1988).
[19] L. Satpathy and R. C. Nayak, At. Data Nucl. Data Tables **39**, 241 (1988); P. Moeller and J. R. Nix, *ibid.* **39**, 213 (1988); E. Comay, I. Kelson, and A. Zidon, *ibid.* **39**, 235 (1988).
[20] D. Vautherin and D. M. Brink, Phys. Rev. C **5**, 626 (1972).
[21] L. D. Miller and A.E.S. Green, Phys. Rev. C **5**, 241 (1972).
[22] R. Brockman and W. Weise, Phy. Rev. C **16**, 1282 (1977).
[23] R. Brockman, Phys. Rev. C **18**, 1510 (1978).
[24] J. P. Elliott and T.H.R. Skyrme, Nuovo Cimento **10**, 164 (1956).
[25] C. J. Horowtiz, in *Relativistic Dynamics and Quark-Nuclear Physics,* edited by M. B. Johnson and A. Picklesimer (Wiley-Interscience, New York, 1986).
[26] J. C. Parikh and J. P. Svenne, Phys. Rev. C **174**, 1343 (1968).
[27] H. J. Flocard, in *Nuclear Self-Consistent Fields,* edited by G. Ripka and M. Porneuf (North-Holland, Amsterdam, 1975).
[28] L. S. Celenza, Shun-fu Gao, and C. M. Shakin, Phys. Rev. C **41**, 1768 (1990).
[29] Sara Cruz-Barrios *et al.*, Phys. Rev. C **43**, 181 (1991).
[30] I. Angeli *et al.*, J. Phys. G **6**, 303 (1980).
[31] J. A. Nolen and J. P. Schiffer, Annu. Rev. Nucl. Sci. **19**, 471 (1969).
[32] H. D. Wohlfahrt *et al.*, Phys. Lett. **73B**, 131 (1978).
[33] P. Moeller and J. R. Nix, Los Alamos National Laboratory Report No. LA-UR-86-3983, 1986.
[34] J. D. Bjorken and S. Drell, *Relativistic Quantum Mechanics* (McGraw-Hill, New York, 1964); J. J. Sakurai, *Advanced Quantum Mechanics* (Addison-Wesley, Reading, 1984).
[35] H. J. Emrich *et al.*, Ref. [11], Vol. I, p. 33.
[36] I. Tanihata, Nucl. Phys. **A522**, 275c (1991).
[37] J. Theis, G. Grabner, G. Buchwald, J. Maruhm, W. Greiner, H. Stocker, and J. Polonyi, Phys. Rev. D **28**, 2286 (1983).
[38] S. J. Lee *et al.*, Phys. Rev. Lett. **57**, 2116 (1986).
[39] S. K. Patra and C. R. Praharaj (unpublished).
[40] H. Toki, Y. Sugahara, D. Hirata, B. V. Carlson, and I. Tanihata, Nucl. Phys. **A524**, 633 (1991).
[41] K. Holinde, Phys. Rep. **68**, 122 (1981).
[42] A. Bouyssy, S. Marcos, and Pham Van Thieu, Nucl. Phys. **A422**, 541 (1984).
[43] J. P. Blaizot, D. Gogny, and B. Grammaticos, Nucl. Phys. **A265**, 315 (1975).
[44] E. F. Serr and J. D. Walecka, Phys. Lett **79B**, 10 (1978).
[45] K. Nakamura, S. Hitamatsu, T. Kamae, and H. Muramatsu, Nucl. Phys. **A271**, 221 (1976); J. Mougoy *et al.*, *ibid.* **A262**, 461 (1979).
[46] G. Ripka, *Advances in Nuclear Physics* (Plenum, New York, 1968), Vol. 1.
[47] S. DeBenedetti, *Nuclear Interactions* (Wiley, New York, 1966), Chap. 6.
[48] H. A. Bethe, Annu. Rev. Nucl. Sci. **21**, 93 (1971).